ELSEVIER

Journal of Organometallic Chemistry 484 (1994) 71–80

Journal of Organometallic Chemistry

Site selectivity in carbon monoxide insertion into a Pt–C σ-bond of the binuclear complex $[(CH_3)ClPt(\mu\text{-}Cl)(\mu\text{-}Ph_2PPy)Pt(CH_3)(DMSO)]DMSO$. Structural characterization of the derivatives $[(CH_3CO)ClPt(\mu\text{-}Cl)(\mu\text{-}Ph_2PPy)Pt(CH_3)(DMSO)]$ and $[(CH_3)ClPt(\mu\text{-}Ph_2PPy)_2Pt(COCH_3)]^+$

Carmela G. Arena [a], Gianfranco Ciani [b], Dario Drommi [a], Felice Faraone [a,*], Davide M. Proserpio [b], Enrico Rotondo [a]

[a] *Dipartimento di Chimica Inorganica, Analitica, e Struttura Molecolare, Università di Messina, Salita Sperone 31, Villaggio S. Agata, 98010 Messina, Italy*

[b] *Istituto di Chimica Strutturistica Inorganica, Università di Milano, via Venezian, 21, 20133 Milano, Italy*

Received 21 February 1994

Abstract

Carbon monoxide reacts with $[(CH_3)ClPt(\mu\text{-}Cl)(\mu\text{-}Ph_2PPy)Pt(CH_3)(DMSO)]DMSO$, **1**, to give $[(CH_3CO)ClPt(\mu\text{-}Cl)(\mu\text{-}Ph_2PPy)Pt(CH_3)(DMSO)]$ **2**. The insertion of CO into a platinum–carbon σ-bond of **1** shows a site selectivity, occurring at the Pt–CH_3 bond involving the metal atom connected to the P atom of the 2-(diphenylphosphino)pyridine (Ph_2PPy). Under a carbon monoxide atmosphere for about 30 h, **1** forms the ionic compound $[(CH_3)ClPt(\mu\text{-}Ph_2PPy)_2Pt(COCH_3)][Pt(CO)(COCH_3)Cl_2]$, **3**. Complex **2** changes slowly into **3**. It was not possible to obtain crystals of **2** or **3** suitable for X-ray investigations. A crystal species was isolated containing both **2** and **3** in a 1:1 ratio. The crystals are triclinic, space group $P\bar{1}$ (no. 2), with $a = 10.326(4)$ Å, $b = 16.648(4)$ Å, $c = 22.203(4)$ Å, $\alpha = 90.95(2)°$, $\beta = 96.50(2)°$, $\gamma = 95.44(2)°$. The refinements, based on 3255 significant reflections, gave a final R value of 0.0621. The molecular structure of the neutral species **2** is similar to that of the parent compound **1**, with a CH_3CO group in place of a methyl. The structure of the anion of **3** was incompletely characterized because of disorder. The $[(CH_3)ClPt(\mu\text{-}Ph_2PPy)_2Pt(COCH_3)]^+$ cation has a direct Pt–Pt bond of 2.728(3) Å bridged by the two Ph_2PPy ligands in a head-to-tail fashion. One of the Pt atoms completes its coordination with an acetyl group and is four-coordinate, whereas the second containing both a chlorine atom and a methyl group, is five-coordinate. Semi-empirical MO calculations for the cation have been performed, and show the dative nature of the $Pt^{II} \rightarrow Pt^{II}$ bond.

Keywords: Platinum; Dinuclear; X-ray structure; EHMO calculations

1. Introduction

In recent years we have been interested in the synthesis of homo- and hetero-bimetallic complexes stabilized by only one "short bite" unsymmetrical bridging 2-(diphenylphosphine)pyridine(Ph_2PPy) [1–10] in contrast to the "A-frame" type compounds. In these species the metal centres are held close together by the geometric requirements of the bridging bidentate Ph_2PPy and this can give rise to transfer of ligands from one metal to the other, intramolecular redox processes, and making or breaking of the metal–metal bond. The presence of only one bridging ligand increases the range of substrates compared with the A-frame compounds, which can reach the metal centres for bimetallic activation.

Recently [10], we reported the reaction of *cis*-$[Pt(DMSO)(Ph_2PPy)Cl_2]$ (DMSO = dimethylsulfoxide) with *cis*-$[Pt(DMSO)_2(CH_3)_2]$. We were able to isolate

* Corresponding author.

SSDI 0022-328X(94)24707-P

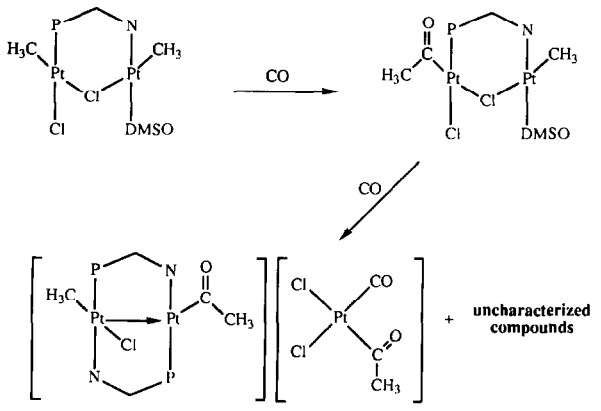

Scheme 1.

only two reaction products, the binuclear platinum (II)–platinum(II) complex $[(CH_3)ClPt(\mu\text{-}Cl)(\mu\text{-}Ph_2PPy)Pt(CH_3)(DMSO)]DMSO$ (**1**) and the binuclear platinum(I)–platinum(I) complex $[Pt_2(\mu\text{-}Ph_2PPy)_2Cl_2]DMSO$. In this paper we report the insertion reaction of CO into one of the Pt–CH_3 bonds of $[(CH_3)ClPt(\mu\text{-}Cl)(\mu\text{-}Ph_2PPy)Pt(CH_3)(DMSO)]DMSO$ (**1**) and the results of an X-ray structure analysis of a crystal containing two derivatives, $[(CH_3CO)ClPt(\mu\text{-}Cl)(\mu\text{-}Ph_2PPy)Pt(CH_3)(DMSO)]$ (**2**) and $[(CH_3)ClPt(\mu\text{-}Ph_2PPy)_2Pt(COCH_3)][Pt(CO)(COCH_3)Cl_2]$ (**3**).

2. Result and discussion

2.1. Synthesis and NMR characterization

The reactions observed are shown in Scheme 1. The stoichiometry is not specified because the reaction produced additional species which were not characterized.

When carbon monoxide was bubbled into a dichoromethane solution of $[(CH_3)ClPt(\mu\text{-}Cl)(\mu\text{-}Ph_2PPy)Pt(CH_3)(DMSO)]DMSO$, **1**, the pale yellow became more intense. The appearance of broad bands at 1663 cm^{-1} and 1690 cm^{-1}, together with a terminal ν(CO) band at 2072 cm^{-1} was observed. Thc band at 1663 cm^{-1} slowly disappeared, while the band at 2072 cm^{-1} and the broad band at 1690 cm^{-1} increased. This broad band results from two close overlapping bands. By slow evaporation of a dichloromethane solution of **1** through which carbon monoxide was bubbled, yellow crystals suitable for X-ray analysis were obtained. Surprisingly, the asymmetric unit contains three different species. The structures of two of these have been fully characterized, namely $[(CH_3CO)ClPt(\mu\text{-}Cl)(\mu\text{-}Ph_2PPy)Pt(CH_3)(DMSO)]$ (**2**) and $[(CH_3)ClPt(\mu\text{-}Ph_2PPy)_2Pt(COCH_3)]^+$ (**3a**), while the third species, a mononuclear Pt complex, was only partially resolved because of a disorder (see below).

The structural characterization of the species **2** and **3a** has been used in the assignments of the NMR resonances and of the characteristic IR bands.

The species **3a** is cationic; the conducting compound **3**, $[(CH_3)ClPt(\mu\text{-}Ph_2PPy)_2Pt(COCH_3)][Pt(CO)(COCH_3)Cl_2]$, containing **3a**, was obtained when CO was slowly bubbled for about 30 h through a dichloromethane solution of **1**. Unfortunately it was not possible to obtain crystals of **3** suitable for X-ray analysis. The anionic part, **3b**, was characterized by IR and NMR data (see below). In the IR spectrum, the terminal ν(CO) band at 2072 cm^{-1} and one of the overlapping $\nu(COCH_3)$ bands at 1690 cm^{-1} are a result of **3b**, while the other $\nu(COCH_3)$ band is consistent with the structure found for **3a**. From these data species **3b** is thought to be the anionic complex $[Pt(CO)(COCH_3)Cl_2]^2$.

A compound which analyzes for **2** was obtained by reducing the reaction time of **1** with CO to a few minutes, but IR and NMR spectra indicated the presence of small amounts of **3**. All attempts to obtain **2** free of **3** failed.

With the aim of obtaining further information on the reaction of **1** with CO, a detailed NMR study was undertaken. Crystals of **1** were dissolved in CD_2Cl_2 and the resulting solution was saturated with CO. The ^1H, $^{31}P\{^1H\}$ and ^{195}Pt NMR spectra of the solution were monitored with time. The spectra of a freshly prepared solution are consistent with the presence of complex **2** together with relatively small amounts of $[(CH_3)ClPt(\mu\text{-}Ph_2PPy)_2Pt(COCH_3)][Pt(CO)(COCH_3)Cl_2]$ (**3**). The ^1H NMR spectrum shows a singlet with ^{195}Pt satellites at $\delta = 0.025$ [^2J(PtH) = 87.3 Hz] for the methyl directly bonded to platinum, a singlet at $\delta = 1.794$ for the coordinated acetyl group (platinum satellites are obscured by close resonances) and two resonances at $\delta = 3.56$ [^3J(PtH) = 23.4 Hz] and $\delta = 3.77$ [^3J(PtH) = 30.3 Hz] for the methyl groups of the coordinated DMSO (intensity ratio 1:1:1:1). In the aromatic region, resonances consistent with the presence of ten protons are observed between 7.1 ppm and 7.9 ppm, while the 4 H of the pyridine ring shows a doublet of doublets with platinum satellites at δ 8.82 [^3J(HH) = 4.2 Hz; ^4J(HH) = 1.5 Hz; ^3J(PtH) = 44.6 Hz]. The $^{31}P\{^1H\}$ NMR spectrum of the same solution shows an intense resonance at $\delta = 10.35$ with two sets of platinum satellites [^1J(PtP) = 5272 Hz; ^3J(PtP) = 76.2 Hz]. The $^{195}Pt\{^1H\}$ NMR shows a doublet at $\delta = 1004.5$ [^1J(PtP) = 5272 Hz] for the platinum bonded to phosphorus, and a broad resonance at $\delta = 653$ for the platinum bonded to the nitrogen atom of the bridging Ph_2PPy. The broadening is probably caused by the quadrupolar ^{14}N nucleus being directly bonded to the ^{195}Pt. The $^{195}Pt\{^1H\}$ NMR spectrum also indicates the presence of a relatively small Pt–Pt coupling in the complex [J(PtPt) = 70 Hz].

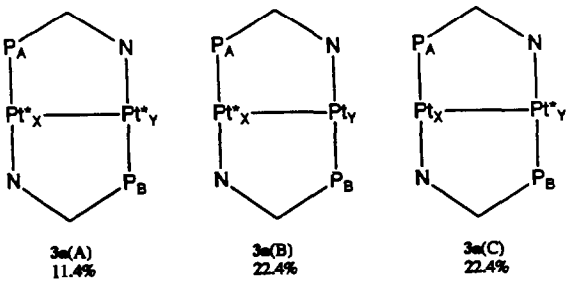

Scheme 2.

Monitoring the NMR spectra showed that a slow process takes place, leading to the complete transformation of **2** into two new species, together with small amounts of other uncharacterized products. The two products, identified as **3a** and **3b**, are also present in the freshly prepared dichloromethane solution, but their concentration increases with time while the concentration of **2** decreases.

The $^{31}P\{^1H\}$ NMR spectrum of the crystals dissolved in CD_2Cl_2 and, left for three days at room temperature in the NMR tube, shows only two resonances (intensity ratio 1:1) at $\delta = 13.75$ [$^1J(PtP) = 4643$ Hz; $^2J(PtP) = 41.7$ Hz] and at $\delta = 9.57$ [$^1J(PtP) = 3592$ Hz; $^2J(PtP) = 122.7$ Hz]. The $^{195}Pt\{^1H\}$ NMR spectrum of the same sample shows resonances that are consistent with the existence of three magnetically active isotopomers (see Scheme 2).

Consistent with the proposed structure, the isotopomer **3a**(A) should show an ABXY spin system. The X part of this system is observed in the $^{195}Pt\{^1H\}$ NMR spectrum as a doublet of doublets of doublets centred at $\delta = 525$ [$^1J(Pt_XP_A) = 3592$ Hz; $^1J(Pt_XPt_Y) = 2440$ Hz; $^2J(Pt_XP_B) = 41$ Hz].

The isotopomer **3a**(B), an ABX spin system, gives a doublet of doublets centred at the same position. The intensities of these two sets of resonances are as expected for the natural abundance of ^{195}Pt (33.8%), and the $^1J(PtP)$ values are equal to that observed for the resonance centred at $\delta = 9.57$ in the $^{31}P\{^1H\}$ NMR spectrum.

The isotopomer **3a**(C), an ABY spin system, gives a broad doublet of doublets at $\delta = 982.2$ [$^1J(Pt_YP_B) = 4635$ Hz; $^2J(Pt_YP_A) = 42$ Hz]. The platinum–phosphorus coupling constants are the same as for the corresponding resonance at $\delta = 13.75$ in the $^{31}P\{^1H\}$ NMR spectrum.

The $^{31}P\{^1H\}$ and $^{195}Pt\{^1H\}$ NMR spectra are consistent with structure **3a** which contains the two platinum and the two phosphorus atoms in magnetically different environments. Although the Pt–Pt couplings are notoriously difficult to interpret [11], the value of 2440 Hz is certainly indicative of a direct metal–metal bond, with a high degree of s character. The absence of a detectable P–P coupling in **3a** may be attributed to the approximately 130° dihedral angle between the Pt–P bonds. The $^3J(PtP)$ coupling of **3a** seems somewhat smaller than those observed in analogous binuclear complexes containing Pt–Pt bonds. In our opinion the values observed may reflect the combination of coupling constants of different sign through the P–Pt–Pt bond and through the P–C–N–Pt bonds.

The ^1H NMR spectra are consistent with a slow reaction that produces **3** from **2**. The spectra show that over three days the resonances of the coordinated DMSO give place to the singlet of free DMSO at $\delta = 2.52$, and that at the same time all the resonances of **2** disappear while the intensity of the resonances attributed to **3a** and **3b** increase. Resonances of many different by-products are also observed in the ^1H NMR spectra. Moreover, the formation of moderate amounts of metallic platinum was observed inside the NMR tube. In order to confirm the proposed reaction pathway, the reaction of **1** and carbon monoxide was performed in the NMR tube using 99% ^{13}CO. The ^1H NMR spectra of the reaction mixture show that **1** is immediately and quantitatively transformed into **2** after addition of carbon monoxide. The acetyl protons (observed as a singlet at $\delta = 1.794$ in the reaction with unenriched CO) show a doublet at $\delta = 1.8$ [$^2J(CH) = 5.7$ Hz].

The $^{13}C\{^1H\}$ NMR spectrum of the same solution shows a doublet at $\delta = 197.9$ [$^2J(CP) = 5.1$ Hz] flanked by platinum satellites [$^1J(PtC) = 935.6$ Hz] which we attribute to the coordinated acetyl. Consistent with the transformation of **2** into **3a** and **3b**, in the $^{13}C\{^1H\}$ NMR spectrum during three days, the doublet at $\delta = 197.9$ nearly disappears, and is replaced by three new doublets, each with platinum satellites, at $\delta = 200.6$ [$^2J(CP) = 4.6$ Hz, $^1J(PtC) = 789$ Hz], at $\delta = 199.6$ [$^2J(CC) = 1.6$ Hz, $^1J(PtC) = 1070$ Hz], and at $\delta = 160.1$ [$^2J(CC) = 1.6$ Hz, $^1J(PtC) = 2225$ Hz]. The last resonance is attributed to a terminal carbonyl of a Pt^{II} derivative. Two-dimensional ^{13}C-^{13}C homonuclear-correlated spectra show cross-peaks between the resonances at $\delta = 160.1$ and that at $\delta = 199.6$ ppm [$^2J(CC) = 1.6$ Hz]. Thus we attribute these two doublets to the acetyl and to the terminal carbonyl, respectively, of **3b** and the doublet at $\delta = 200.6$ to the acetyl of **3a**. The NMR parameters of **3b** are different to those reported [12] for the anion $[Pt(CO)(CH_3)Cl_2]^-$. This further supports the structure assigned to anion **3b**.

2.2. X-ray structural characterization of the complexes 2 and 3a

Triclinic yellow crystals were always obtained from the reaction whatever the reaction time and conditions. The crystal contains discrete neutral molecules of $[(COCH_3)ClPt(\mu\text{-}Cl)(\mu\text{-}Ph_2PPy)Pt(CH_3)(DMSO)]$ (**2**), cations $[(CH_3)ClPt(\mu\text{-}Ph_2PPy)_2Pt(COCH_3)]^+$ (**3a**)

and mononuclear anions *cis*-$[Pt(CO)(COCH_3)Cl_2]^-$ (**3b**), in the ratio 1:1:1, which exhibit normal van der Waals contacts. Unfortunately the anions **3b**, lying in large cavities among the bulkier dinuclear species, are disordered, as shown by the high atomic thermal parameters (all greater than 11.0 Å^2), which prevented a complete structural characterization. It was possible to refine only a square planar *cis*-$[PtX_2Cl_2]^-$, with X = C, with two Pt–Cl bonds both of 2.30(2) Å and two Pt–C bonds of 2.24(7) Å and 2.16(7) Å and bond angles all close to 90° or 180°. Probably the disorder also involves positional exchange between the carbonyl and the acetyl groups.

2.3. Structure of $[(COCH_3)ClPt(\mu\text{-}Cl)(\mu\text{-}Ph_2PPy)Pt(CH_3)(DMSO)]$ (2)

The neutral dinuclear species **2** is illustrated in Fig. 1.

The two platinum atoms display square planar geometries, and are bridged by Ph_2PPy and Cl1. The structure is similar to that of the parent compound $[(CH_3)ClPt(\mu\text{-}Cl)(\mu\text{-}Ph_2PPy)Pt(CH_3)(DMSO)]$ (**1**), except for the presence of a terminal acetyl group replacing a methyl group on Pt2A, the metal atom bearing the terminal chlorine atom and which is bound to the P atom of the Ph_2PPy bridge. Selected bond distances and angles are reported in Table 1, and are compared with the corresponding values in **1** [11], which have smaller uncertainties. The Pt · · · Pt nonbonding contact is slightly longer in **2** than in **1**, 3.378(2) Å versus 3.3075(6) Å. For the other bond parameters the differences, even when significant, are small.

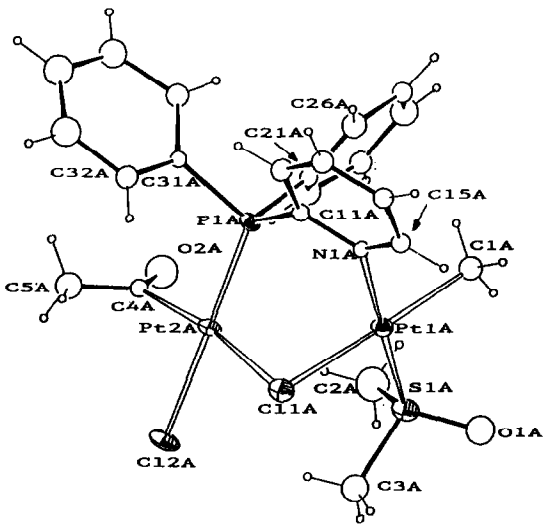

Fig. 1. ORTEP drawing of $[(COCH_3)ClPt(\mu\text{-}Cl)(\mu\text{-}Ph_2PPy)Pt(CH_3)(DMSO)]$ (**2**). For clarity only two carbon atoms of each ring are labelled.

The coordination of the acetyl group is as expected, with the plane defined by the atoms of this ligand

Table 1
Selected bond parameters for $[(COCH_3)ClPt(\mu\text{-}Cl)(\mu\text{-}Ph_2PPy)Pt(CH_3)(DMSO)]$ (**2**). The corresponding values for compound **1** are in square brackets

Distances (Å)					
Pt1A · · · Pt2A	3.378(2)	[3.3075(6)]	S1A–O1A	1.48(4)	[1.46(1)]
Pt1A–S1A	2.20(1)	[2.194(3)]	S1A–C2A	1.76(5)	[1.78(1)]
Pt1A–Cl1A	2.42(1)	[2.428(3)]	S1A–C3A	1.75(4)	[1.76(1)]
Pt1A–N1A	2.07(3)	[2.063(9)]	C4A–O2A	1.28(5)	–
Pt1A–C1A	2.11(4)	[2.04(1)]	C4A–C5A	1.36(6)	–
Pt2A–Cl1A	2.47(1)	[2.477(2)]	P1A–Cl1A	1.86(4)	[1.832(8)]
Pt2A–Cl2A	2.34(1)	[2.356(3)]	P1A–C21A	1.82(4)	[1.81(1)]
Pt2A–P1A	2.20(1)	[2.183(2)]	P1A–C31A	1.83(4)	[1.81(1)]
Pt2A–C4A	2.01(4)	[2.05(1)] [a]			
Angles (°)					
Cl1A–Pt1A–C1A	175(1)	[173.5(3)]	Pt1A–S1A–C3A	112(2)	[108.2(5)]
Cl1A–Pt1A–N1A	85.7(7)	[83.9(2)]	O1A–S1A–C2A	109(2)	[107.0(7)]
Cl1A–Pt1A–S1A	95.8(4)	[96.03(9)]	O1A–S1A–C3A	108(2)	[107.6(6)]
C1A–Pt1A–N1A	90(1)	[89.6(4)]	C2A–S1A–C3A	99(2)	[101.1(8)]
C1A–Pt1A–S1A	89(1)	[90.5(4)]	Pt1A–N1A–C11A	120(2)	[121.6(6)]
S1A–Pt1A–N1A	178.5(8)	[178.6(2)]	Pt1A–N1A–C15A	119(2)	[117.4(7)]
Cl1A–Pt2A–Cl2A	88.7(4)	[87.28(9)]	Pt2A–C4A–C5A	122(3)	–
Cl1A–Pt2A–P1A	94.4(4)	[97.32(9)]	Pt2A–C4A–O2A	117(3)	–
Cl1A–Pt2A–C4A	171(1)	[175.1(3)] [a]	C5A–C4A–O2A	121(4)	–
Cl2A–Pt2A–P1A	176.6(4)	[174.8(1)]	Pt2A–P1A–Cl1A	117(1)	[114.0(3)]
Cl2A–Pt2A–C4A	85(1)	[88.1(4)] [a]	Pt2A–P1A–C21A	118(1)	[116.0(3)]
P1A–Pt2A–C4A	92(1)	[87.4(4)] [a]	Pt2A–P1A–C31A	112(1)	[114.4(3)]
Pt1A–Cl1A–Pt2A	87.4(4)	[84.81(8)]	Cl1A–P1A–C21A	100(2)	[102.5(4)]
Pt1A–S1A–O1A	117(1)	[119.7(4)]	Cl1A–P1A–C31A	104(2)	[103.8(4)]
Pt1A–S1A–C2A	111(2)	[111.6(5)]	C21A–P1A–C31A	104(2)	[104.7(4)]

[a] For the methyl carbon atom in compound **1**.

almost perpendicular to the plane of the Pt2A square planar environment [dihedral angle between the "best planes" of 79(1)°]. The C4A atom exhibits the largest out-of-plane displacement from the (Pt2A, Cl1A, Cl2A, P1A, C4A) best plane (ca. 0.20 Å).

The Ph_2PPy twist about the Pt–Pt axis is demonstrated by the value of the P1A–Pt2A–Pt1A–N1A torsion angle, 35.1(8)°, almost identical to the corresponding parameter in **1**.

2.4. Structure of $[(CH_3)ClPt(\mu\text{-}Ph_2PPy)_2Pt(COCH_3)]^+$ (3a)

The structure of **3a** is shown in Fig. 2. Selected bond distances and angles are given in Table 2.

The dinuclear complex exhibits a direct metal–metal interaction of 2.728(3) Å. This Pt–Pt bond is bridged by two Ph_2PPy ligands, head-to-tail (HT), which form two pairs of Pt–P and Pt–N bonds *trans* at Pt2B and *cis* at Pt1B. The coordination around Pt2B is completed by an acetyl ligand *trans* to the Pt–Pt vector [Pt–Pt–C 173(1)°], while that around Pt1B is completed by a methyl group and terminal chlorine atom *cis* to it.

The Pt2B atom is therefore in a square planar environment, somewhat distorted as shown by the interligand angles in the range 86–96°, and the out-of-plane displacements of the individual atoms from the "best plane" (Pt2B, Pt1B, P2b, N1B, C2B), between ca. −0.13 Å and +0.18 Å, for C2B and N1B respectively. The acetyl group, as in **2**, is almost perpendicular to the above plane [dihedral angle between the "best planes" of 74(3)°].

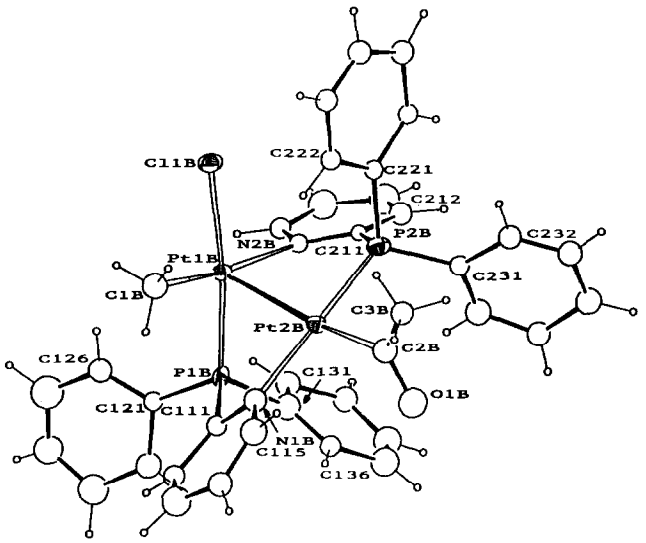

Fig. 2. ORTEP drawing of the cation $[(CH_3)ClPt(\mu\text{-}Ph_2PPy)_2Pt(COCH_3)]^+$ (**3a**). For clarity only two carbon atoms of each ring are labelled.

Table 2
Selected bond parameters of $[(CH_3)ClPt(\mu\text{-}Ph_2PPy)_2Pt(COCH_3)]^+$ (**3a**)

Distances (Å)			
Pt1B–Pt2B	2.728(3)	C2B–C3B	1.53(6)
Pt1B–P1B	2.19(1)	C2B–O1B	1.24(6)
Pt1B–Cl1B	2.31(1)	P1B–C111	1.83(4)
Pt1B–C1B	1.90(4)	P1B–C121	1.78(4)
Pt1B–N2B	2.15(3)	P1B–C131	1.83(5)
Pt2B–P2B	2.21(1)	P2B–C211	1.77(4)
Pt2B–C2B	1.92(5)	P2B–C221	1.82(4)
Pt2B–N1B	2.08(3)	P2B–C231	1.76(4)
Angles (°)			
P1B–Pt1B–Pt2B	74.7(3)	Pt1B–P1B–C131	117(2)
P1B–Pt1B–Cl1B	172.8(4)	Pt1B–N2B–C211	126(3)
P1B–Pt1B–C1B	90(1)	Pt1B–N2B–C215	115(3)
P1B–Pt1B–N2B	97.9(8)	Pt2B–P2B–C211	109(1)
Cl1B–Pt1B–Pt2B	111.9(3)	Pt2B–P2B–C221	114(1)
Cl1B–Pt1B–C1B	87(1)	Pt2B–P2B–C231	115(1)
Cl1B–Pt1B–N2B	85.7(8)	Pt2B–N1B–C111	116(3)
C1B–Pt1B–Pt2B	96(1)	Pt2B–N1B–C115	126(3)
C1B–Pt1B–N2B	172(1)	Pt2B–C2B–C3B	121(3)
N2B–Pt1B–Pt2B	85.2(9)	Pt2B–C2B–O1B	121(4)
P2B–Pt2B–Pt1B	86.1(3)	C3B–C2B–O1B	118(4)
P2B–Pt2B–C2B	89(1)	C111–P1B–C121	105(2)
P2B–Pt2B–N1B	173(1)	C111–P1B–C131	108(2)
C2B–Pt2B–Pt1B	173(1)	C121–P1B–C131	102(2)
C2B–Pt2B–N1B	96(2)	C211–P2B–C221	108(2)
N1B–Pt2B–Pt1B	90(1)	C211–P2B–C231	102(2)
Pt1B–P1B–C111	111(1)	C221–P2B–C231	108(2)
Pt1B–P1B–C121	113(1)		

A square pyramidal or incomplete octahedral five-fold coordination is observed around Pt1B. The P1B, N2B, Cl1B and C1B atoms give rise to an irregular square-planar coordination. These atoms have smaller deviations from the relevant "best plane" than those around Pt2B, the maximum displacement being ca. 0.11 Å for Cl1B. The angles at Pt1B involving these atoms vary from 85.7(8)° (Cl1B–Pt1B–N2B) to 97.9(8)° (P1B–Pt1B–N2B).

The structure of **3a** is rather unusual. The complex belongs to a small family of about ten members of dinuclear compounds, held together by bridging ligands, characterized by the presence of a direct metal–metal bond joining a square-planar to a square-pyramidal frame. The family includes homonuclear Pt–Pt [13,14] and Rh–Rh [15–18] species and heteronuclear Pt–Pd [19] and Pt–Rh [20] ones. The more popular bonding model for these complexes implies a M → M dative bond from the five-coordinate metal atom to the four coordinate, and will be discussed in detail below.

The metal atoms in this family of complexes are bridged by two tridentate ligands in all but one case [18], which contains only one tridentate bridging group. The bridging ligands employed posses either equal or different donor atoms. Rigid bridges such as 1-methylcytosinate [19] and benzothiazole-2-thiolate [20] give *trans–trans* head-to-head (HH) coordination. Symmet-

ric bridging ligands, such as $[Ph_2PCH_2PPh_2]$ [14] and $[(PhO)_2PN(Et)P(OPh)_2]$ [15], give a *trans–cis* coordination, with two P atoms *trans* in the square-planar frame and two P atoms *cis* in the square-pyramidal.

Complex **3a** is the first example within this family to contain bridging 2-(diphenylphosphino)pyridine, though many dinuclear species have been reported with this short-bite ligand. In particular, closely related complexes are the mixed-metal species $[(CO)Cl_2Rh(\mu\text{-}Ph_2PPy)_2PdCl]$ [21] and $[(CO)_2ClRu(\mu\text{-}Ph_2PPy)_2PdCl]$ [22], in which the Pd atoms are square-planar while the other metal atoms are octahedral, the two bridging Ph_2PPy showing a head-to-tail (HT) *trans–cis* coordination, as in **3a**. The HT coordination is that more frequently encountered in dinuclear species doubly bridged by Ph_2PPy, but examples of the HH type have also been reported, e.g. in $[ClPt(\mu\text{-}Ph_2PPy)_2(\mu\text{-}CO)Mo(CO)_2Cl]$ [23].

The P1B–Pt1B–Pt2B–N1B and P2B–Pt2B–Pt1B–N2B torsion angles, −45(1)° and 29.6(9)°, respectively, have values inside the range observed in complexes with Ph_2PPy bridging ligands. Because of different intramolecular steric factors, the Ph_2PPy twist about the metal–metal axis can decrease to ca. 21° in $[(CO)Cl_2Rh(\mu\text{-}Ph_2PPy)_2PdCl]$ [21], or increase to ca. 47° in $[(CO)_2ClRu(\mu\text{-}Ph_2PPy)_2PdCl]$ [22], with respect to a central value (between 30° and 40°) which is related to the intrinsically preferred conformation of the aromatic rings of the ligand. The most frequent conformations of the phenyl rings in the strictly related PPh_3 fragment are in fact those with approximate C_3 symmetry and torsion angles of 40° [24].

The Pt1B–Pt2B bond [2.728(3) Å] is significantly longer than the corresponding metal–metal interaction of 2.5853(6) Å in $[ClPt(\mu\text{-}Ph_2PPy)_2PtCl]$ [11], containing two HT bridging ligands. It is more similar to the Pt–Pt bond of 2.769(1) Å in $[MePt(\mu\text{-}Ph_2PCH_2PPh_2)_2PtMe_2]^+$ [14], the unique, other member of the same family containing two platinum atoms, not considering $[Pt_2(CH_3)_2(\mu\text{-}C_5H_4PPh_2)_2]$ which contains a π-bonded cyclopentadienyl fragment [25]. The Pt–Pt vector in **3a** deviates significantly from the direction of the normal to the "best plane" of the square-planar environment around Pt1B, 20.2(3)° versus a value of 9° in $[MePt(\mu\text{-}Ph_2PCH_2PPh_2)_2PtMe_2]^+$. As a consequence, the P1B–Pt1B–Pt2B and N2B–Pt1B–Pt2B angles are acute [74.7(3)° and 85.2(9)°], while the C1B–Pt1B–Pt2B and C11B–Pt1B–Pt2B angles are obtuse [96(1)° and 111.9(3)°].

The Pt–Cl, Pt–P and Pt–N bond distances are normal, while the Pt–C bonds are somewhat shorter than expected, but uncertainties are too large for detailed discussion.

2.5. Bonding within the complex 3a

The nature of the metal–metal bond in homonuclear [14–18] and heteronuclear [18–20] dimers idealized as $(D_{4h})L_4M\text{–}ML_3(C_{2v})$ has been described as a dative (or the equivalent donor-acceptor) metal–metal bond [14,26]. We have analyzed this in detail using extended Hückel theory [27]. First we constructed the molecular orbitals (MO) of the complex and the fragment molecular orbitals (FMO) interaction diagram in terms of $(D_{4h})L_4M$ and $ML_3(C_{2v})$. Fig. 3 shows the metal centred FMOs for the two fragments of an ideal $Pt_2H_7^{3-}$-I (see, for example, page 340 of ref. [28]). Seven AOs of the two metals are engaged in M–L bonds and two p orbitals lie unperturbed at high energy (typical of square-planar 16-electron complexes). The interactions of the remaining nine FMOs give rise to 8 MOs with Pt–Pt bonding-antibonding character and one lone-pair (d_x^2 in Fig. 3) centred on the Pt of the T-shaped fragment. Filling these orbitals with 16 electrons results in a net single σ metal–metal bond.

Moving to a more realistic model such as $[Pt_2(NH_2)_2(PH_3)_2MeCl(COMe)]^-$ **II**, but still without bridging ligands to allow straightforward FMO analysis, introduces a great deal of orbital mixing. The lone-pair and the σ interaction redistribute over different MOs without changing the result of a net single bond. Calculations of different geometries, from eclipsed to staggered, showed that the metal–metal bond, because of the σ symmetry of the interaction, is

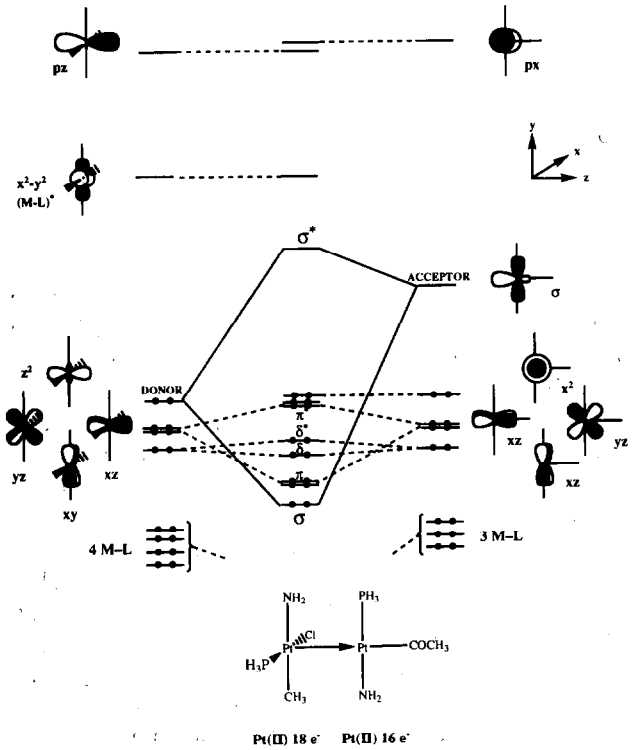

Fig. 3. Molecular orbitals interaction diagram for the model $Pt_2H_7^{3-}$ (I).

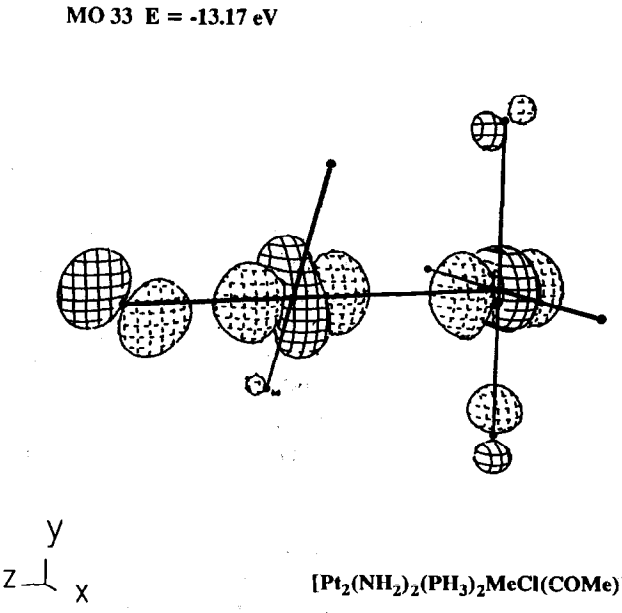

Fig. 4. CACAO plot[35] of the MO with Pt–Pt σ-bond character for the model compound $[Pt_2(NH_2)_2(PH_3)_2MeCl(COMe)]^-$ (II).

not directly affected by rotations, and so the torsion of the two fragments observed in **3a** should be the result of steric interactions. Fig. 4 shows the MO which contributes most to the Pt–Pt bond for staggered model **II**, here the bond interaction is delocalized over MeOC–Pt–Pt. Calculations with the experimental geometry of **3a** do not change the nature of the Pt–Pt interaction.

Let us consider the two possible descriptions of the bond, dative and covalent. Computation of the electronic population of the FMOs for the staggered model **II** shows the populations of the donor-acceptor levels in the molecule to be 1.8 and 0.2 electrons, respectively. This small transfer is consistent with the heuristic description of the dative bond as a donation of a pair of electrons from one centre to the other (with ideal occupations of 2 and 0).

A possible isomer of **3a** could have the methyl group *trans* to a P atom. Calculations on **II** show that the observed molecule with the chlorine *trans* to the phosphine is the most stable, probably because of the stabilization of a π donor (Cl) with the π acceptor phosphine.

3. Conclusions

CO "insertion" into metal–carbon σ-bond is a key step in practical CO-based synthesis, but it has been difficult to study in detail, especially with complexes that involve rather labile intermediates [29].

The study of the reaction of complex **1** with CO is relevant to the understanding of the reactivity and site-selectivity exhibited by binuclear complexes, particularly in CO "insertion" reactions into a metal–carbon σ-bonded species. The reaction of **1** with CO is very complex, as shown by monitoring the reaction course by NMR spectroscopy and as indicated by the nature of the isolated products. Compound **2** appears as the result of CO insertion into a Pt–CH_3 σ-bond of **1** at the metal centre at which the coordination is completed by the phosphorus atom of Ph_2PPy, plus terminal and bridging chloride. Thus, the CO "insertion" reaction exhibits a site selectivity at this metal centre.

Several reaction schemes have been proposed for carbonyl "insertion" reactions at square-planar complexes [30]. They reflect the relative importance of the electronic and steric properties of the neutral L (usually tertiary phosphine) and of the anionic organic ligand R in determining the reaction intermediate and thus the reaction course.

Early reports on CO "insertion" into metal–carbon σ-bond in mononuclear complexes of the type $[MRXL_2]$ (M = Pd or P, X = halogenide, L = tertiary phosphine) indicate that these took place from five-coordinate intermediates [30–32]. In principle, the uptake of CO by a tri-coordinated platinum(II) species formed in a dissociative pathwise cannot be ruled out [33].

We may also assume that the reaction of **1** with CO leads initially to the five-coordinate adduct $[(CH_3)(CO)ClPt(\mu\text{-}Cl)(\mu\text{-}Ph_2PPy)Pt(CH_3)DMSO]$ which subsequently evolves to give **2**, either by direct migratory insertion of the CH_3 group or by the formation of a four-coordinate intermediate, possibly via the chloride bridge-splitting reaction. It is noteworthy that the site selectivity occurs at the platinum centre bonded through phosphorus to Ph_2PPy, and not at the other Pt bearing the labile DMSO molecule. This seems to be the result of a kinetic effect because of the ability of the soft phosphorus atom to facilitate the uptake of CO and the formation of the five-coordinate species. In complex **1** the Pt(1)–CH_3 and Pt(2)–CH_3 bond distances of 2.05(1) Å and 2.04(1) Å compare well and, furthermore, these two bonds are both *trans* to the bridging chlorine. This seems to rule out the possibility that the site selectivity is a result of a differential lability of these ligands.

The formation of **3** from **2** is a very complex process. The mechanism of this reaction is quite obscure because it implies a complete redistribution of ligands. The structural characterization of the cation offers a new insight in the chemistry of dinuclear metal complexes containing short-bite bridging ligands.

4. Experimental details

The compound $[(CH_3)ClPt(\mu\text{-}Cl)(\mu\text{-}Ph_2PPy)Pt(CH_3)(DMSO)]DMSO$ (**1**) was prepared as described

previously [10]. All other reagents were purchased and used as supplied. Solvents were dried by standard procedures. All experiments were performed under purified dinitrogen. IR spectra were obtained as Nujol mulls on KBr or CsI plates using a Perkin-Elmer FTIR 1720 spectrophotometer. NMR spectra were recorded on a Bruker WP80-SY or on a Bruker 300 AMX-R spectrometers. ^{1}H, and ^{13}C NMR spectra are referenced to internal tetramethylsilane (TMS), ^{31}P spectra to external 85% H_3PO_4, ^{195}Pt chemical shifts are given in absolute frequency assuming TMS = 100 MHz, positive chemical shifts are for all nuclei to higher frequency of the reference. Conductivity measurements were made with a Radiometer CDM 3 conductivity meter. Molecular weights were determined with a Knauer vapor pressure osmometer. Elemental analyses were performed by REDOX s.n.c., Codogno M., Milano.

4.1. Reaction of $[(CH_3)ClPt(\mu\text{-}Cl)(\mu\text{-}Ph_2PPy)Pt(CH_3)(DMSO)]DMSO$ (1) with CO

Carbon monoxide was bubbled into a dichloromethane solution (20 mL) of **1** (0.080 g, 0.088 mmol) for about 10 min. The solution was then reduced in volume to ca. 5 mL and diethyl ether (30 mL) was added to give a yellow solid. This was filtered off and washed with diethyl ether. Analytical data are in accordance with the formulation $[(CH_3CO)ClPt(\mu\text{-}Cl)(\mu\text{-}Ph_2PPy)Pt(CH_3)(DMSO)]$ **2**, but NMR spectra indicate that the product contains small amounts of $[(CH_3)ClPt(\mu\text{-}Ph_2PPy)_2Pt(COCH_3)][Pt(CO)(COCH_3)Cl_2]$ **3**. All the attempts to obtain **2** free of **3** failed. Anal. Calc. for $C_{22}H_{26}Cl_2NO_2PPt_2S$: C, 30.71; H, 3.05; N, 1.63; Cl, 8.24. Found: C, 31.29; H, 2.85; N, 1.68; Cl, 8.94.

4.2. Preparation of $[(CH_3)ClPt(\mu\text{-}Ph_2PPy)_2Pt(COCH_3)][Pt(CO)(COCH_3)Cl_2]$ (3)

A dichloromethane solution (20 mL) of **1** (0.090 g, 0.099 mmol) was saturated with CO and left to stand for about 30 h. During this time the solution turned from pale yellow to yellow. The volume of solution was then reduced to ca. 5 mL, and diethyl ether (30 mL) was added to precipitate a yellow solid. The crude product was treated with methanol to give a yellow solution; the product **3** was obtained by adding diethyl ether. Yield 51% (0.045 g, 0.033 mmol). $\Lambda = 98\ \Omega^{-1}\ cm^2mol^{-1}$ for 5.10^{-4}–10^{-4} M solution in methanol. Anal. Calc. for $C_{40}H_{37}Cl_3N_2O_3P_2Pt_3$: C, 35.66; H, 2.77; N, 2.08; Cl, 7.89. Found: C, 35.69; H, 2.79; N, 2.09; Cl, 7.94%. A solution of **2** in CH_2Cl_2 slowly gives **3** even in the absence of free CO.

4.3. X-ray data collection

Crystal data are reported in Table 3.

The crystal sample was mounted on a glass fibre in air. The intensity data were collected on an Enraf-Nonius CAD4 automated diffractometer using graphite monochromatized Mo–Kα radiation. The setting angles of 25 random intense reflections [$16° < 2\theta < 25°$] were used in both cases to determine by least-squares fit accurate cell constants and the orientation matrix. The collection was performed by the ω-scan method, within the limits $6° < 2\theta < 48°$. A variable scan-speed and a variable scan-range were used, with a 25% extension at each end of the scan-range for background determination. Three standard intense reflections, monitored every 2 h, showed crystal decay of ca. 15% at the end of the collection. The intensities were corrected for Lorentz, polarization, and decay effects. An empirical absorption correction was applied to the data, based on ψ-scans (ψ 0–360° every 10°) of three suitable reflections with χ values close to 90°. The number of significant [$I > 3\sigma(I)$] independent reflections used in the structure solution and refinements was 3255.

Table 3
Crystal data and intensity collection parameters

Formula	$C_{62}H_{63}Cl_5N_3O_5P_3Pt_5S$
FW, amu	2207.89
System	triclinic
Space group	$P\bar{1}$ (No. 2)
a, Å	10.326(4)
b, Å	16.648(4)
c, Å	22.203(4)
α, °	90.95(2)
β, °	96.50(2)
γ, °	95.44(2)
V, Å^3	3774(2)
D_c, g cm^{-3}	1.943
Z	2
$F(000)$	2064
Radiation	Mo–Kα, λ = 0.71073 Å
μ(Mo–Kα)	96.43
Min. transmission factor	0.61
Crystal dimensions, mm	0.10×0.15×0.22
Crystal decay	15%
Scan mode	ω
ω-scan width, °	1.20+0.35 tan θ
θ-range, °	3–24
Temperature, °C	22±2
Octants of reciprocal space	$\pm h, \pm k, +l$
Measured reflections	11771
No. of reflections with $I > 3\sigma(I)$	3255
Final R and R_w indices	0.0621, 0.0603
No. of refined variables	395

$R = \Sigma F_0 - kF_c / \Sigma F_0$ $R_w = [\Sigma w(F_0 - kF_c)^2 / \Sigma w F_0^2]^{1/2}$

Table 4
Final positional and thermal parameters

Atom	x	y	z	B (Å²)
Pt1A	−0.3800(2)	0.2558(1)	0.53740(8)	3.57(5) [a]
Pt2A	−0.4827(2)	0.3269(1)	0.40031(8)	3.26(5) [a]
P1A	−0.299(1)	0.3929(6)	0.4420(5)	3.2(3) [a]
Cl1A	−0.579(1)	0.3113(6)	0.4971(5)	4.4(3) [a]
Cl2A	−0.672(1)	0.2545(7)	0.3510(6)	5.9(4) [a]
S1A	−0.447(1)	0.1302(7)	0.5095(6)	4.8(3) [a]
O1A	−0.421(3)	0.068(2)	0.555(1)	6.9(8)
C1A	−0.202(3)	0.216(2)	0.577(2)	5(1)
C2A	−0.385(5)	0.103(3)	0.442(2)	9(2)
C3A	−0.614(4)	0.118(3)	0.483(2)	6(1)
C4A	−0.432(3)	0.343(2)	0.316(2)	2.6(8)
C5A	−0.487(5)	0.397(3)	0.278(2)	6(2)
O2A	−0.355(3)	0.295(2)	0.298(1)	9.1(8)
C11A	−0.294(3)	0.430(2)	0.522(2)	2.6(8)
C12A	−0.271(4)	0.512(2)	0.539(2)	3.9(9)
C13A	−0.259(4)	0.533(3)	0.596(2)	4(1)
C14A	−0.274(3)	0.477(2)	0.640(2)	3.4(8)
C15A	−0.303(3)	0.394(2)	0.619(2)	3.0(8)
N1A	−0.312(2)	0.374(2)	0.564(1)	2.1(6)
C21A	−0.151(3)	0.342(2)	0.448(2)	2.8(8)
C22A	−0.133(4)	0.279(3)	0.408(2)	6(1)
C23A	−0.024(4)	0.235(2)	0.420(2)	4(1)
C24A	0.075(5)	0.260(3)	0.461(2)	6(1)
C25A	0.066(3)	0.325(2)	0.497(2)	3.3(8)
C26A	−0.044(4)	0.363(3)	0.489(2)	5(1)
C31A	−0.256(3)	0.484(2)	0.401(2)	2.3(7)
C32A	−0.347(4)	0.536(2)	0.391(2)	4.1(9)
C33A	−0.320(5)	0.603(3)	0.353(2)	7(1)
C34A	−0.206(5)	0.616(3)	0.325(2)	7(1)
C35A	−0.115(5)	0.563(3)	0.337(2)	6(1)
C36A	−0.132(4)	0.495(2)	0.377(2)	4.3(9)
Pt1B	0.0372(2)	0.9438(1)	0.89515(8)	3.45(5) [a]
Pt2B	0.1462(2)	0.9269(1)	0.78991(8)	3.56(5) [a]
P1B	−0.120(1)	0.8831(7)	0.8306(5)	3.6(3) [a]
P2B	0.212(1)	1.0569(7)	0.8012(5)	4.9(3) [a]
Cl1B	0.188(1)	1.0010(8)	0.9727(5)	5.6(3) [a]
C1B	0.075(4)	0.842(2)	0.926(2)	6(1)
O1B	0.179(3)	0.913(2)	0.668(2)	8.3(9)
C2B	0.239(5)	0.924(3)	0.720(2)	6(1)
C3B	0.388(4)	0.921(2)	0.727(2)	5(1)
C111	−0.064(4)	0.794(2)	0.795(2)	4.0(9)
C112	−0.131(4)	0.719(3)	0.790(2)	5(1)
C113	−0.057(5)	0.658(4)	0.766(2)	8(2)
C114	0.054(5)	0.675(3)	0.743(2)	6(1)
C115	0.118(5)	0.744(3)	0.755(2)	7(1)
N1B	0.062(3)	0.808(2)	0.780(2)	5.2(9)
C121	−0.260(4)	0.846(2)	0.865(2)	3.6(9)
C122	−0.373(5)	0.814(3)	0.829(2)	6(1)
C123	−0.489(6)	0.780(3)	0.853(3)	9(2)
C124	−0.491(6)	0.786(3)	0.912(3)	8(1)
C125	−0.378(6)	0.805(3)	0.947(3)	11(2)
C126	−0.262(5)	0.833(3)	0.921(2)	5(1)
C131	−0.191(5)	0.944(3)	0.770(2)	7(1)
C132	−0.267(4)	1.006(3)	0.791(2)	6(1)
C133	−0.307(4)	1.063(3)	0.745(2)	6(1)
C134	−0.288(5)	1.047(3)	0.687(3)	8(1)
C135	−0.219(5)	0.989(3)	0.669(3)	8(1)
C136	−0.169(4)	0.930(3)	0.712(2)	4(1)
C211	0.089(3)	1.107(2)	0.831(2)	2.5(8)
C212	0.064(4)	1.185(3)	0.820(2)	5(1)
C213	−0.025(5)	1.226(4)	0.846(3)	9(2)
C214	−0.093(5)	1.187(4)	0.887(3)	9(2)
C215	−0.075(4)	1.106(3)	0.896(2)	4(1)

Table 4 (*continued*)

Atom	x	y	z	B (Å²)
N2B	0.017(3)	1.066(2)	0.868(1)	3.3(7)
C221	0.364(4)	1.080(2)	0.851(2)	3.5(9)
C222	0.422(4)	1.023(3)	0.882(2)	4(1)
C223	0.535(4)	1.042(3)	0.921(2)	5(1)
C224	0.578(4)	1.117(3)	0.932(2)	6(1)
C225	0.526(4)	1.183(3)	0.907(2)	5(1)
C226	0.413(4)	1.162(2)	0.865(2)	3.8(9)
C231	0.227(4)	1.108(2)	0.733(2)	4(1)
C232	0.345(4)	1.142(3)	0.714(2)	5(1)
C233	0.357(5)	1.178(3)	0.662(2)	6(1)
C234	0.252(5)	1.183(3)	0.622(2)	7(1)
C235	0.130(5)	1.146(3)	0.639(2)	6(1)
C236	0.123(5)	1.115(3)	0.695(2)	7(1)
Pt1C	0.3284(3)	0.5929(2)	0.1913(1)	11.2(1) [a]
Cl1C	0.113(2)	0.571(1)	0.2101(9)	12.2(7) [a]
Cl2C	0.352(2)	0.715(1)	0.2435(9)	14.0(8) [a]
C1C	0.312(7)	0.473(4)	0.143(3)	13(2)
C2C	0.527(7)	0.609(4)	0.169(3)	13(2)

[a] Equivalent isotropic *B* factor.

4.4. Structure solution and refinements

The data reduction was performed on a PDP 11/73 computer, using the Enraf-Nonius Structure Determination Package (SDP) and the physical constants tabulated therein. All the other crystallographic computations were carried out by using the SHELX programs.

The structure was solved by direct methods, which revealed the locations of the Pt atoms. Successive difference Fourier maps highlighted the locations of the non-hydrogen atoms. Other than two ordered dinuclear Pt complexes, another mononuclear species was found, consisting of a central Pt atom surrounded in a square-planar fashion, by two *cis* chlorine atoms and two lighter atoms, which were treated as carbon atoms. Difference Fourier maps performed after many cycles of refinement showed many residual peaks around this fragment, especially close to the two carbon atoms, but it was not possible to refine any further atom or atom fraction. Attempts to refine disorder models, based on a possible interchange between a CO and a $COCH_3$ group, were all unsuccessful.

The refinements were carried out by block-matrix least-squares, with three blocks, one for each molecular fragment, minimizing the function $\Sigma w(F_o - k|F_c|)^2$. Anisotropic thermal parameters were assigned to the Pt, Cl, P and S atoms.

The hydrogen atoms of the ordered complexes were located in ideal positions (C–H 0.95 Å) after each cycle of refinement but not refined; their thermal B parameters were fixed to 6.0 Å^2.

The final difference-Fourier map showed residual peaks not exceeding ca. 2 e Å^{-3}, close to the $[PtCl_2C_2]$ fragment.

Weights were assigned according to the formula $w = k/[\sigma^2(F_o) + gF_o^2]$, with $k = 1.5182$ and $g = 1.326 \times 10^{-3}$. The final values of the conventional agreement indices R and R_w are reported in Table 3. The final positional and isotropic thermal parameters are given in Table 4.

Anisotropic thermal factors, the calculated fractional coordinates of the hydrogen atoms and a complete list of bond distances and angles have been deposited with the Cambridge Crystallographic and Data Centre, and these and a structure factor table are also available from the authors.

4.5. Computational details

We used the extended Hückel method [27], a semiempirical molecular orbital procedure, with weighted H_{ij} [34], as implemented in CACAO [35]. The parameters used in the calculations are taken from ref. [36]. The geometry of model **II** is based on the structure of **3a**.

Acknowledgements

We thank the Consiglio Nazionale delle Ricerche (CNR) Progetto Finalizzato Chimica Fine II for financial support.

References

[1] G. Bruno, S. Lo Schiavo, E. Rotondo, C.G. Arena and F. Faraone, *Organometallics*, *8* (1989) 886.
[2] E. Rotondo, S. Lo Schiavo, A. Bruno, C.G. Arena, R. Gobetto and F. Faraone, *Inorg. Chem.*, *28* (1989) 2944.
[3] S. Lo Schiavo, F. Faraone, M. Lanfranchi and A. Tiripicchio, *J. Organomet. Chem.*, *387* (1990) 357.
[4] S. Lo Schiavo, E. Rotondo, G. Bruno and F. Faraone, *Organometallics*, *10* (1991) 1631.
[5] S. Gladiali, L. Pinna, C.G. Arena, E. Rotondo and F. Faraone, *J. Mol. Cat.*, *66* (1991) 183.
[6] E. Rotondo, G. Battaglia, C.G. Arena and F. Faraone, *J. Organomet. Chem.*, *419* (1991) 399.
[7] C.G. Arena, E. Rotondo, F. Faraone, M. Lanfranchi and A. Tiripicchio, *Organometallics*, *10* (1991) 3877.
[8] C.G. Arena, F. Faraone, M. Lanfranchi, E. Rotondo and A. Tiripicchio, *Inorg. Chem.*, *31* (1992) 4797.
[9] G. De Munno, G. Bruno, C.G. Arena, D. Drommi and F. Faraone, *J. Organomet. Chem.*, *451* (1993) 263.
[10] C.G. Arena, G. Bruno, G. De Munno, E. Rotondo, D. Drommi and F. Faraone, *Inorg. Chem.*, *32* (1993) 1601.
[11] P.S. Pregosin, *Coord. Chem. Rev.*, *44* (1982) 1601.
[12] J. Browning, P.L. Goggin, R.J. Goodfellow, N.W. Hurst, L.G. Mallison and M. Murray, *J. Chem. Soc., Dalton Trans.*, (1978) 872.
[13] A.A. Frew, L. Manojlovic-Muir and K.W. Muir, *J. Chem. Soc., Chem. Commun.*, (1980) 624.
[14] M.P. Brown, S.J. Cooper, A.A. Frew, L. Manojlovic-Muir, K.W. Muir, R.J. Puddephatt, K.R. Seddon and M.A. Thompson, *Inorg. Chem.*, *20* (1981) 1500.
[15] R.J. Haines and E. Meintjies, *Inorg. Chim. Acta*, *36* (1979) L403.
[16] M.P. Anderson and L.H. Pignolet, *Organometallics*, *2* (1983) 1246.
[17] J.A. Ladd, M.M. Olmstead and A.L. Balch, *Inorg. Chem.*, *23* (1984) 2318.
[18] H. El-Amouri, A.A. Bahsoun, J. Fischer and J.A. Osborn, *Angew. Chem., Int. Edn. Engl.*, *26* (1987) 1169.
[19] M. Krumm, B. Lippert, L. Randaccio and E. Zangrando, *J. Am. Chem. Soc.*, *113* (1991) 5129; M. Krumm, E. Zangrando, L. Randaccio, S. Menzer and B. Lippert, *Inorg. Chem.*, *32* (1993) 700.
[20] M.A. Ciriano, J.J. Perez-Torrente, F.J. Lahoz and L.A. Oro, *Inorg. Chem.*, *31* (1992) 969.
[21] J.P. Farr, M.M. Olmstead and A.L. Balch, *J. Am. Chem. Soc.*, *102* (1980) 6654; J.P. Farr, M.M. Olmstead and A.L. Balch, *Inorg. Chem.*, *22* (1983) 1229.
[22] A. Maisonnet, J.P. Farr, M.M. Olmstead, C.T. Hunt and A.L. Balch, *Inorg. Chem.*, *21* (1982) 3961.
[23] J.P. Farr, M.M. Olmstead, N.M. Rutherford, F.E. Wood and A.L. Balch, *Organometallics*, *2* (1983) 1758.
[24] E. Bye, B.W. Schweizer and J.D. Dunitz, *J. Am. Chem. Soc.*, *104* (1982) 5893.
[25] M. Lin, K.A. Fallis, G.K. Anderson, N.P. Rath and M.Y. Chiang, *J. Am. Chem. Soc.*, *114* (1992) 4687.
[26] MO calculation of a dative metal–metal bond in L_5M–$M'L_5$ have been reported by H. Nakatsuji, M. Hada and A. Kawashima, *Inorg. Chem.*, *31* (1992) 1740.
[27] R. Hoffmann and W.N. Lipscomb, *J. Chem. Phys.*, *36* (1962) 2179, 2872; R. Hoffmann, *J. Chem. Phys.*, *39* (1963) 1397.
[28] T.A. Albright, J.K. Burdett and M.-W. Whangbo, *Orbital Interactions in Chemistry*, John Wiley & Sons, New York, 1985.
[29] G.W. Parshall and S.D. Ittel, *Homogeneous Catalysis* 2 edn., John Wiley & Sons, New York, 1992, p. 93; F. Calderazzo, *Angew. Chem., Int. Edn. Engl.*, *16* (1977) 299.
[30] G.K. Anderson and R.J. Cross, *Acc. Chem. Res.*, *17* (1984) 67.
[31] C. Booth and J. Chatt, *J. Chem. Soc., A* (1966) 634; H.F. Kleim, *Angew. Chem., Int. Edn. Engl.*, *12* (1973) 402.
[32] P.E. Garrou and R.F. Heck, *J. Am. Chem. Soc.*, *98* (1976) 4115.
[33] R. Romeo, *Comments Inorg. Chem.*, *11* (1990) 21.
[34] J.H. Ammeter, H.-B. Bürgi, J.C. Thibeault and R. Hoffmann, *J. Am. Chem. Soc.*, *100* (1978) 3686.
[35] C. Mealli and D.M. Proserpio, *J. Chem. Ed.*, *66* (1990) 399.
[36] H. Summerville and R. Hoffmann, *J. Am. Chem. Soc.*, *98* (1976) 7240.